Nuclear Materials and Energy 30 (2022) 101139

Contents lists available at ScienceDirect

Nuclear Materials and Energy

journal homepage: www.elsevier.com/locate/nme

An *in-situ* ToF-LEIS and AES study of near-surface modifications of the composition of EUROFER97 induced by thermal annealing

Jila Shams-Latifi [a,*], Petter Ström [a], Eduardo Pitthan [a], Daniel Primetzhofer [a,b]

[a] Department of Physics and Astronomy, Division of Applied Nuclear Physics, Uppsala University, Box 516, SE-751 20 Uppsala, Sweden
[b] Tandem Laboratory, Uppsala University, Box 529, SE-751 21 Uppsala, Sweden

ARTICLE INFO

Keywords:
EUROFER97
ToF-LEIS
AES
In-situ
Annealing
Segregation
Diffusion

ABSTRACT

Surface segregation and diffusion of W, Ta, Cr, O and S after thermal annealing of EUROFER97 were studied *in-situ*. The sample was prepared by polishing, annealing up to 300°C and 3 keV Ar sputtering. *In-situ* measurements with time-of-flight low energy ion scattering using 8 keV Ne ions and Auger electron spectroscopy were carried out close to room temperature after each annealing, in sequence, to 425°C, 675°C, 400°C, 675°C, 900°C, and 925°C. Surface segregation/diffusion of chromium and tungsten and/or tantalum can be observed in the ion scattering spectra. The segregation of sulfur was clearly observed in Auger electron spectroscopy. The energy converted time-of-flight low-energy ion scattering spectrum after the first annealing to 675°C was compared to Monte-Carlo simulations using the TRBS code. The most compatible simulation indicates a layer enriched in W + Ta of 1 ± 0.3 nm featuring 0.0276 combined relative concentration of tungsten and tantalum to total metal content which is considerably higher than the bulk value of 0.0042.

Introduction

EUROFER97 is a reduced activation ferritic martensitic (RAFM) steel developed in Europe as a structural material to be used in the breeding blanket of envisioned future fusion machines and possibly in a demonstration reactor (DEMO). The maximum operating temperature of EUROFER97 has been specified as approximately 550°C. For further details on operation conditions for EUROFER97, see [1]. However, transient events such as edge localized modes (ELMs) [2] may at least temporarily raise the temperature of the first wall, and structural materials immediately behind it, above 550°C [3]. Additionally, proposals for breeding blankets in fusion devices include designs, where EUROFER97 parts are covered with thin oxide dispersion strengthened (ODS)-EUROFER steel plates or even completely replaced [4]. In such scenarios, the breeding blanket lifetime would be extended and the maximum operating temperature would be increased to about 650°C. It has been observed [3,5], when both increasing the operating temperature and maintaining EUROFER97 as a structural material, processes occurring in that material above 550°C become relevant for the design of components and lead to segregation of its alloying elements, chromium, tungsten and tantalum, to the surface of the material and grain boundaries. In the case of application of EUROFER97 as plasma-facing material, segregation of heavy components (W, Ta) due to the increased working temperature might have positive effects on e.g. its durability. In both experimental and computational studies [6,7] it has been shown that the presence of tungsten atoms at the surface of the first wall significantly reduces the wall erosion rate due to preferential sputtering, and prolongs the time needed to erode through a given material thickness. As a consequence of the same physical process, i.e. preferential sputtering, the surface of EUROFER97 is expected to deviate from bulk composition upon plasma exposure. The evolution of the near-surface composition of EUROFER97 due to preferential sputtering and thermal annealing has been investigated as a function of both ion irradiation parameters and temperature by different ion beam-based analytical techniques such as low-energy ion scattering using an electrostatic analyser (ESA-LEIS) [8], time-of-flight medium-energy ion scattering (ToF-MEIS) [9], and recently by *in-situ* Rutherford backscattering (RBS) [3]. Thermally-induced segregation is studied for EUROFER97 without involving preferential sputtering in [3]. The depth resolution achieved in the RBS-measurements in that work was not enough to resolve where the segregated atoms are located. ESA-LEIS, in turn, provides superior surface sensitivity, the information depth, however, is limited [10]. Finally, the resolution achievable in ToF-MEIS [11] could set limits for the thickness of the segregation region but not yet determine the exact

* Corresponding author.
E-mail address: jila.shams@physics.uu.se (J. Shams-Latifi).

https://doi.org/10.1016/j.nme.2022.101139
Received 17 December 2021; Received in revised form 9 February 2022; Accepted 15 February 2022
Available online 17 February 2022

thickness of the layer.

In this work, *in-situ* time-of-flight low-energy ion scattering (ToF-LEIS) is employed to study the evolution of the near-surface composition of EUROFER97 induced by thermal annealing to temperatures up to 925°C in various steps. The advantage of this method over ToF-MEIS and RBS is its higher surface sensitivity and depth resolution, with larger probing depth than achievable in ESA-LEIS at, however, reduced sensitivity. Specifically, ToF-LEIS can achieve close to monolayer resolution in the near-surface region but probe several nanometers below the surface [12] which enables pinpointing the exact composition profile of the near-surface enrichment in heavy elements observed for EUROFER97 undergoing thermal annealing.

Experiment

Sample preparation

A 10 × 10 mm^2 sample of EUROFER97 with a thickness of 1 mm was polished following the method employed in [9] with minor changes to the lapping material grain size sequence and excluding vacuum baking. The sample was mounted in the analysis chamber (ANA) [13] of the low-energy ion scattering setup, ACOLISSA [14] at Uppsala University. To remove residual surface contaminations affecting the ultimate surface sensitivity of the ToF-LEIS measurements [15], additional surface cleaning was performed using a 3 keV argon beam at a grazing angle of 30° with a total fluence of 4.05 × 10^{14} mm^{-2}. The sputtering was complemented with thermal annealing of the sample to approximately 300°C for 20–30 min. Between each annealing and sputtering step, complementary Auger electron spectroscopy (AES) using a 3 keV primary electron beam was performed, with the main aim of assessing possible surface contaminants and light constituents of the sample, as well as getting a qualitative assessment of the near-surface composition. As Fig. 1 shows, the cleaning procedure started with an AES measurement and sequentially annealing, AES and sputtering. This 4-step cycle was repeated until AES showed a minimal amount of C and O contaminants for two subsequent measurements, finishing with an Ar-sputtering step. Calculating the equilibrium surface fraction of W and Fe [16] according to their sputter yields by 3 keV Ar ions reveals that the as-prepared surface was not expected to be noticeably enriched in W due to the preferential sputtering: an assumed sputter yield of 2 atoms/ion for Fe and 1.5 atoms/ion for W, for 3 keV Ar ions [17], result in a W surface fraction of about 0.006 which is only slightly higher than the bulk fraction.

Thermal treatments

Following the *in-situ* preparation, the sample was transferred in ultra-high vacuum to the scattering chamber (ACOLISSA [14]). This setup provides a set of two microchannel plates in a chevron stack configuration to detect the backscattered projectiles at a fixed central angle of θ = 129° and a solid angle coverage of 2 × 10^{-4} sr. The recorded ToF-LEIS spectra were subsequently energy converted.

To study the as-prepared surface, 2 keV He and 8 keV Ne primary ion beams were used in normal incidence geometry. Thereafter, the sample went through several annealing steps to different temperatures. A filament with a nominal power of 35 W and an electron bombardment heating system were used to anneal the sample, enabling the control over the temperature by regulating the filament voltage and/or electron bombardment high voltage. The temperature measurement was performed by three different methods: i) a K-type (chromel–alumel) thermocouple connected to the sample holder for temperatures up to 500°C with an uncertainty of ± 20°C by considering the contribution stemming from the fluctuations in the displayed temperature on the thermocouple reader, as well as fitting uncertainty in the calibration of the thermocouple [18], ii) comparison to the standard forging colours for the temperatures in the range of 500–700°C with an estimated uncertainty of about ± 25°C, and iii) an optical pyrometer (Keller Mikro PV11) observing the light emitted from the sample surface at higher temperatures with an estimated uncertainty of ± 5°C considering adjustment accuracy and eventual slight temperature gradients across the sample. The reason for employing several temperature measurements is that above 500°C the thermocouple reading was considered to be no longer representative of the temperature at the surface of the sample, due to increasing temperature gradients which may differ from those occurring during calibration. In addition, the light emitted from the sample between 500 and 700°C was below the detection limit of the pyrometer.

To reach an equilibrium state, every annealing step was maintained for approximately one hour before turning off the heating systems. The pressure in ACOLISSA during the ToF-LEIS measurements was in the range of 1–3 × 10^{-9} mbar, and the pressure in ANA during the thermal treatments varied between 1 × 10^{-9} and 1 × 10^{-7} mbar, due to outgassing from the sample and its holder. As illustrated in Fig. 1, the sample was annealed to 425°C before the first annealing to 675°C (referred to here as 675°C-1), 400°C, 900°C, 675°C (675°C-2) and 925°C as the last treatment prior to 2 keV He and 8 keV Ne ToF-LEIS measurements. Each annealing step was followed by measuring a ToF-LEIS spectrum using 8 keV Ne ions and AES. The reason for selecting Ne over He primary ions for the measurements in between the annealing steps is found in better mass resolution enabling straightforward separation of iron and chromium signals in addition to the combined signal of tungsten and tantalum. Increased electronic and nuclear stopping powers in the case of Ne compared to He [19] further yield a higher near-surface resolution, even despite increased straggling.

Experimental results

The AES results obtained during sample preparation and the thermal treatments are presented in Fig. 2. The as-polished spectrum shows a significant amount of carbon and oxygen on the surface of the sample. After one sample preparation step (annealing to 300°C + sputtering) surface contamination was reduced, and after five steps, C and O contaminants were no longer detectable while the intensity of the low-

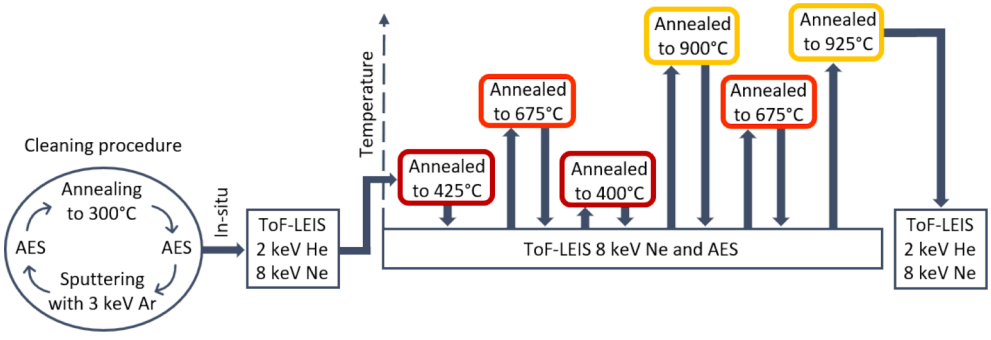

Fig. 1. Flowchart illustrating sample preparation and analysis in this study (AES: Auger Electron Spectroscopy).

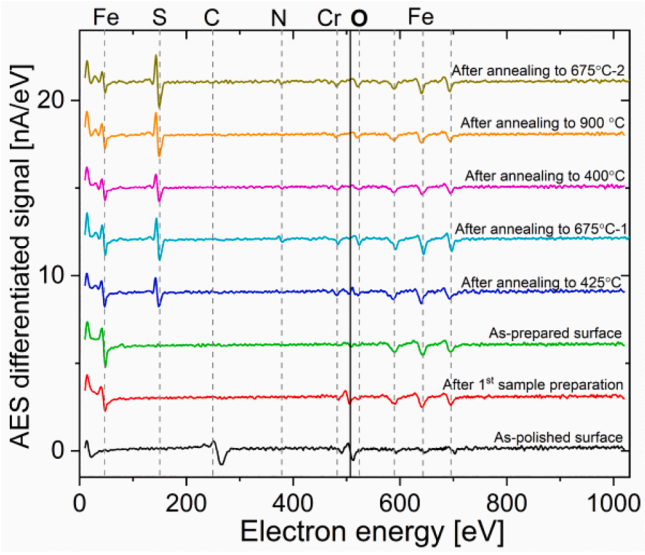

Fig. 2. AES spectra recorded for EUROFER97 at different stages of the present study. Sample preparation steps consist of annealing to 300°C + sputtering. The first and second annealing to 675°C are represented by 675°C-1 and 675°C-2, respectively. Surface segregation of Cr and S is apparent from the spectra recorded after the annealing steps. Due to the low relative elemental sensitivity factor of AES for the expected tungsten signals at 169, 179 and 1736 eV [21], possible enrichment could not be detected for the present integration times. For further details, see the text.

energy lines of iron had increased, indicating a clean surface. During the thermal treatments, sulfur segregates to the surface, presumably from reservoirs in the grain boundaries, which is a known phenomenon in metal alloys [20]. Chromium segregation can also be observed. Because of the low relative elemental sensitivity factor of AES for the expected tungsten signals at 169, 179 and 1736 eV [21], possible enrichment cannot be detected from the AES spectra for the present integration times.

In Fig. 3.a and 3.b, energy converted ToF-LEIS spectra obtained from the as-prepared surface of EUROFER97 using 2 keV He and 8 keV Ne beams are shown. For all energy converted ToF-LEIS spectra presented in this paper, the vertical grey dashed/solid lines determine the position of the surface peak of each element calculated by the corresponding kinematic factors. Due to inelastic losses, which for backscattered ions have been shown to be on the order of several ten eV [22], there exists an uncertainty in the absolute peak position, which is, however, expected to be similar for all species and not affecting unambiguous identification. Moreover, all spectra have been normalized to the spectrum recorded after the first annealing to 675°C. The surface peaks originate from single scattering of the incoming ions from the target atoms at the surface of the sample. The tail signal at higher energies than the surface peaks, which was visible in all the measured spectra, originates from multiple in-plane scattering events [23,24]. The background at energies lower than the surface peak comes from backscattering in deeper layers. One can observe a more pronounced surface peak due to the higher electronic and nuclear stopping powers for 8 keV Ne ions in comparison to 2 keV He ions as well as different scattering kinematics (compare e.g. Fig. 5 in [23]). In addition, the inset of Fig. 3.b offers the logarithmic scale version of the same spectrum. The spectra in Fig. 3.a and 3.b indicate no visible surface peaks for Cr, W and/or Ta on the as-prepared surface which are in good agreement with observations in the AES spectrum "as-prepared" in Fig. 2 indicating Fe as the major detectable element on the sample surface.

As a consequence of thermal treatments, surface segregation/diffusion of chromium and tungsten and/or tantalum can be observed in the normalized energy converted spectra using 8 keV Ne projectiles, in Fig. 4.a and 4.b respectively. It is seen in Fig. 4.a and 4.b, respectively, that after the first annealing to 675°C (675°C-1), Cr (Fe) signal sharply rises (falls) along with significant growth in W + Ta signal. The specific evolution of these surface peaks is described in further detail below.

In Fig. 5, the intensities of Fe, Cr and W + Ta peaks have been analyzed for all the thermal treatment steps by subtracting the background contribution from Fe and Cr peaks for each spectrum. Fig. 5.a exemplifies the employed background subtraction for the 675°C-1 spectrum. Two fixed energy intervals at energies below and above the Cr peak and Fe peak, respectively, were selected to define a linear background to be subtracted from the 1.7–2.6 keV interval of the spectrum. This method has been earlier applied to subtract contributions due to multiple scattering for single-crystalline surfaces yielding a good approximation for the expected single scattering yields [25]. The absolute intensities of Fe, Cr and W + Ta peaks as a function of temperature as well as in chronological order are plotted in Fig. 5.b and 5.c, representations that allow observing potential memory effects. Their relative intensities compared to the sum of Fe, Cr and W + Ta intensities in each step are shown in chronological order in Fig. 5.d. In Fig. 5.b to d, one can follow the evolution of the intensity of Fe, Cr and W + Ta peaks through all the thermal treatment steps. Starting with the annealing to 425°C, in

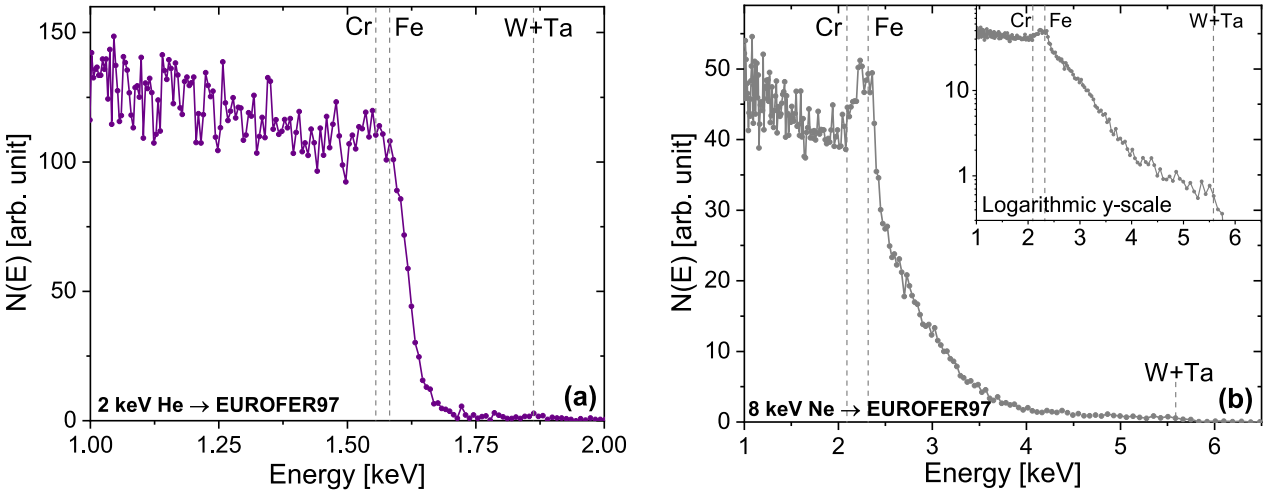

Fig. 3. Energy converted ToF-LEIS spectrum from the as-prepared EUROFER97 surface using a) 2 keV He and b) 8 keV Ne projectiles. The vertical grey dashed lines determine the position of the surface peak of each element calculated by the corresponding kinematic factors. For more details see the text.

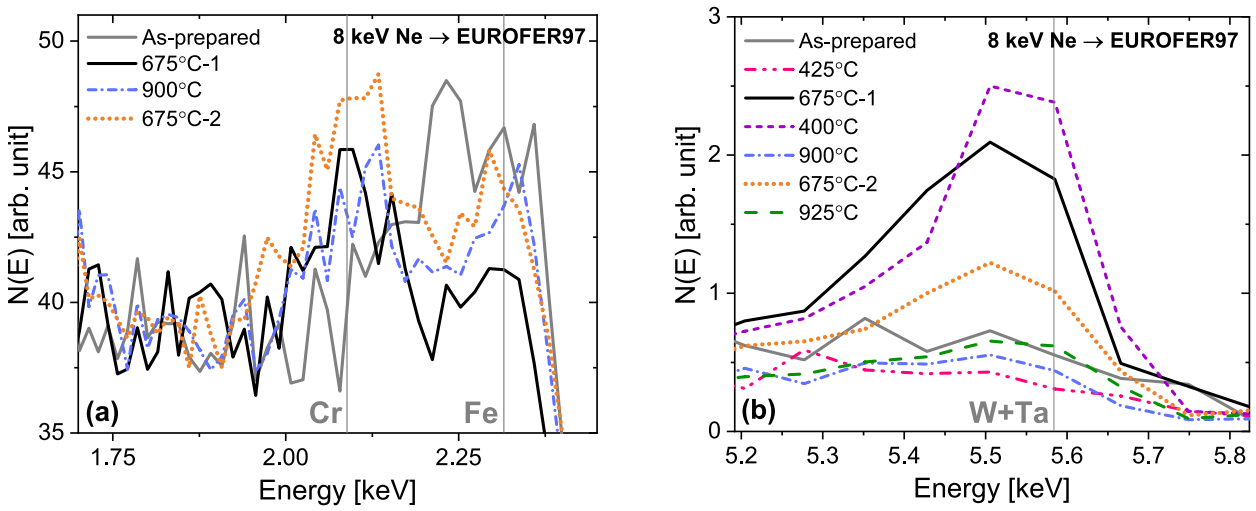

Fig. 4. Evolution of the near-surface signal due to a) iron and chromium and b) tungsten and/or tantalum after different thermal treatments by comparing the corresponding energy converted ToF-LEIS spectra. The vertical grey lines determine the position of the surface peak of each element calculated by the corresponding kinematic factors. Spectra were normalized to the spectrum recorded after the first annealing to 675°C. For more details see the text.

Fig. 5.b(5.c), the intensity of all these three peaks decreases, whereas in Fig. 5.d the relative intensity of Cr slightly increases which means Cr intensity has decreased less than Fe and W + Ta. After annealing to 675°C for the first time (675°C-1), in both Fig. 5.b to d, the intensity of W + Ta almost triples. This increase is also observed in Fig. 5.b to d for Cr, although to a lesser extent in addition to a steep decline in Fe. In the next step, after annealing to 400°C, all intensities (Fe, Cr and W + Ta) show a minor increase in Fig. 5.b(5.c). However, in Fig. 5.d, Cr and W + Ta relative intensities show a minor decrease with a slight rise in that of Fe. By subsequently increasing the temperature to 900°C, the W + Ta intensity drops drastically along with a steep fall in Cr and a minor increase in Fe, Fig. 5.b(5.c). Similarly, Fig. 5.d shows a significant decrease in the W + Ta relative intensity accompanied by a slight reduction in Cr and a notable increase in Fe relative intensities. After increasing the temperature to 675°C for the second time (675°C-2), in Fig. 5.b(5.c), the W + Ta and Cr intensities grow again significantly, with a slight rise in Fe. Whereas, Fig. 5.d indicates a noticeable decline in Fe relative intensity next to the notable growth in the W + Ta and Cr relative intensities. In the end, after annealing to 925°C, again a similar behaviour in Fig. 5.b to d is observed in analogy to the first high-temperature annealing (900°C). Both absolute and relative intensities of Cr and W + Ta decrease, while the intensity of Fe increases. Note, that the ToF-LEIS spectra were not measured during each annealing step but subsequently, while the sample was close to room temperature. In other words, the annealing temperatures shown in Fig. 5.b to d were not achieved in a direct sequence, but the sample was repeatedly cooled down before the next annealing step.

Data analysis, simulations and discussion

The results from Figs. 4 and 5 indicate the presence of both segregation and interdiffusion in certain temperature regions for EUROFER97. This observation is in agreement with the hypothesis presented in earlier studies that were mainly focused on investigating the effects of preferential sputtering, and thermal annealing during sputtering [3,8,9]. In Ström et al. [3], by annealing the sample to 1280°C with various steps in between, it has been claimed that segregation is prominent between 630°C and 830°C, while diffusion brings the surface closer to the bulk composition both above and below this temperature interval. By following the evolution of the relative intensities of Cr and W + Ta peaks in Fig. 5.c, one can find 400°C, 425°C, 900°C and 925°C as the temperatures where the diffusion process is dominant while at 675°C thermally induced segregation prevails, consistent with the proposed claim. Moreover, these remarks agree with the results measured at elevated temperatures in [8] and [9]. In [8] the sample was irradiated with increasing fluences at different temperatures up to 530°C with no indication of W surface enrichment in the corresponding ESA-LEIS spectra using 1 keV primary He ions. In other words, not only there was a lack of thermal enrichment, but also the enrichment related to preferential sputtering was suppressed by diffusion.

The general reduction in the intensity of Fe, Cr and W + Ta peaks all together after the 425°C step in Fig. 5.b and 5.c can be explained by the segregation of lighter elements such as sulfur and oxygen to the surface. Note that both S and O are clearly visible in the corresponding AES in Fig. 2. Other studies have provided a similar observation for phosphorus [26,27]. Increasing the temperature to 675°C for the first time causes segregation of W + Ta and Cr (Fig. 5.b to d) as well as S to the surface of the sample, in addition to the loss of a part of oxygen at the surface (see Fig. 2 as well). After annealing to 400°C, AES indicates a loss of oxygen as compared to the previous steps and diffusion of some S into the bulk (Fig. 2). The AES after annealing to 900°C shows further segregation of S to the surface (Fig. 2). Also, the observed diffusion of W + Ta and Cr (Fig. 5.b to d) is consistent with the suggested diffusion dominancy for metal components at this temperature. In the next step, after annealing for the second time to 675°C, the spectrum in Fig. 2 suggests that the maximum segregation point for S was passed during the decreasing ramp from 900°C so that still a large S peak is visible in AES. Also, the state of the alloy appears to move towards the segregation-dominated region for W + Ta and Cr by a notable rise in their absolute and relative intensities.

In order to extract quantitative information from experimental spectra, simulations were performed for different target compositions. Fig. 6 draws a comparison between the experimental energy spectrum after the 675°C-1 step and its corresponding Monte-Carlo simulations using the TRBS code [28]. The W + Ta region is magnified in the figure inset. The experimental energy spectrum for the as-prepared surface (Fig. 3.b) is also presented to highlight the surface segregation of W + Ta, Cr and S after annealing.

In the simulations, the Molière potential was employed with Firsov screening length corrected according to YTK theory [29] by considering the shell effect of the electron distribution. Thus, a screening correction factor of 0.72 was selected to simulate the interaction between 8 keV Ne ions and the sample constituents. The simulations were performed for 400 million projectiles. The outputs were convolved by a Gaussian

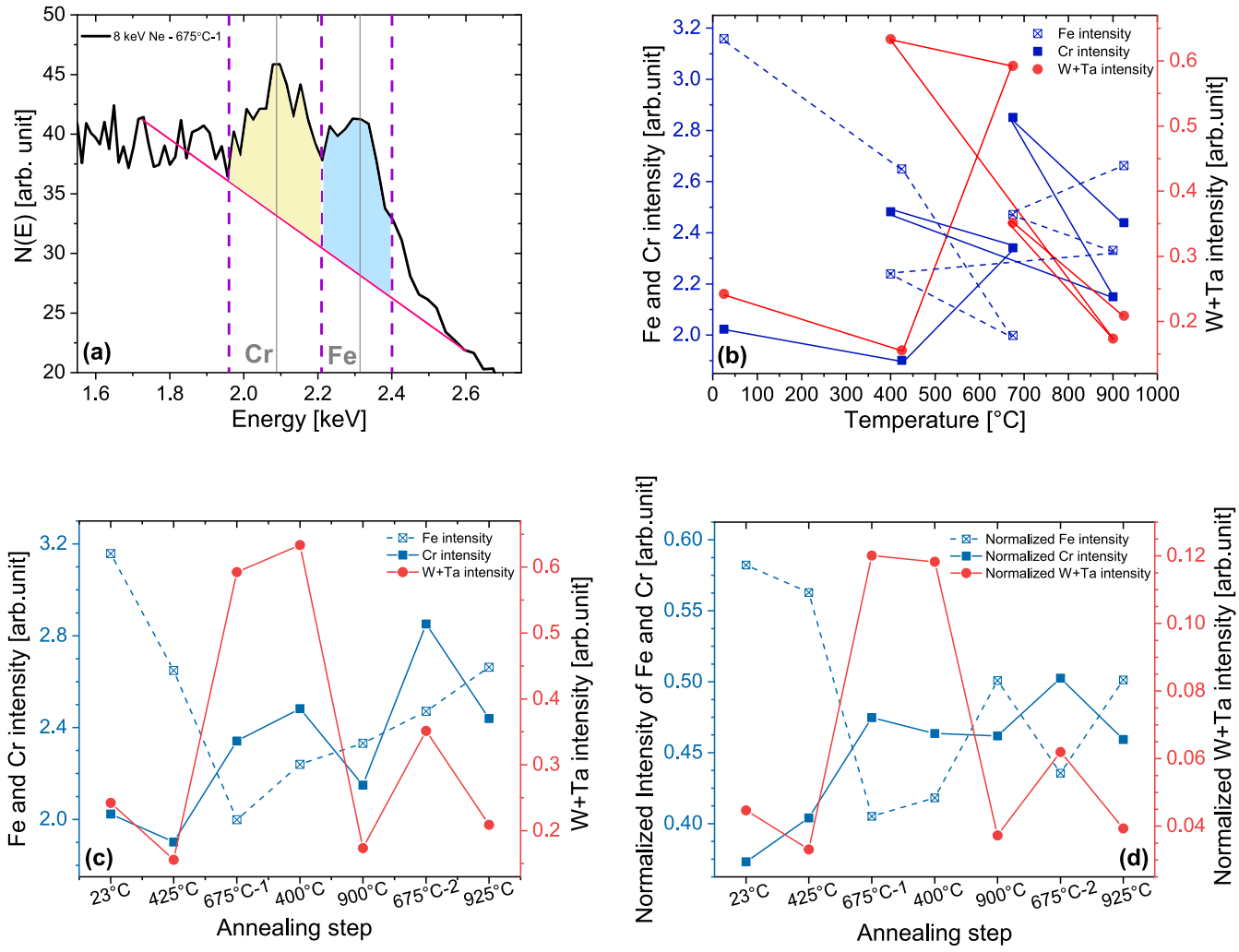

Fig. 5. a) Analysis of the Fe-Cr peak intensity by subtracting the background: the spectrum recorded for the sample annealed for the first time to 675°C, serves as an example, to illustrate the procedure to subtract the background contribution from multiple scattering. The yellow and blue shaded areas indicate the deduced intensity for Cr and Fe for this spectrum, respectively. b) Absolute intensity of Fe, Cr (blue squares, left y-axis) and W + Ta (red circle, right y-axis) peaks vs. temperature of annealing steps in this study. c) the same data as in b) only in chronological order. d) Relative intensity of Fe, Cr (blue squares, left y-axis) and W + Ta (red circle, right y-axis) peaks compared to the sum of their intensities in each annealing step in chronological order. (For interpretation of the references to colour in this figure legend, the reader is referred to the web version of this article.)

function with full width at half maximum (FWHM) equivalent to 80 ns in the time domain to account for detector timing resolution. The details concerning the simulations in Fig. 6 can be found in Table 1. Note that the density of each layer is calculated according to the method proposed in [16] by considering the natural density of a pure bulk of each element weighted by their atomic fraction in that layer. This way, the corresponding thickness of each layer will be as appears in Table 1. In the case of oxide layers, the oxygen density was substituted by that of iron scaled by the atomic mass ratio, thus using the simplifying assumption that O atoms replace Fe while maintaining the average interatomic distance. As TRBS employs the binary collision approximation and non-local electronic energy loss, no effects of density are expected when areal densities are conserved [28]. The bulk composition was taken from [30]. The TRBS simulation "1 nm" is achieved as the most compatible one, showing there is a 1 ± 0.3 nm W + Ta enriched layer containing 0.0276 (W + Ta)/(W + Ta + Fe + Cr) which is considerably higher than their bulk fraction of 0.0042 [9]. From the W + Ta signal at lower energies that attributed to surface single scattering, this simulation also indicates that, in addition to the first enriched layer, another layer exists with 0.0094 (W + Ta)/(W + Ta + Fe + Cr), a fraction slightly higher than the bulk. The uncertainty in the thickness of the enriched layer roots mainly in potential inaccuracies of electronic and nuclear stopping powers, as well as to a more minor degree the scattering potential in the present energy regime. As a result, the TRBS simulation "1 nm" gives an integral near-surface enrichment of W + Ta equivalent to 1.36×10^{14} excess atoms/cm^2 in comparison to the bulk (0.0042 W + Ta of total metals). The simulations "0.5 nm", "1.5 nm", "3.8 nm" and "0.5 nm-conserved" were run to enable a comparison between different possible scenarios. Simulations "0.5 nm" and "1.5 nm" consist of the first enriched layer of 0.5 nm and 1.5 nm, respectively, without keeping the number of excess W + Ta atoms/cm^2 fixed and with the same compositions as TRBS "1 nm", as illustrated in Table 1. Simulation "3.8 nm" comprises only one enriched layer of 3.8 nm, and simulation "0.5 nm-conserved" shows a structure again with the first enriched layer of 0.5 nm, by preserving the number of excess W + Ta atoms/cm^2, see again Table 1. The integral thickness of enrichment equivalent to 3.8 nm was chosen to match the

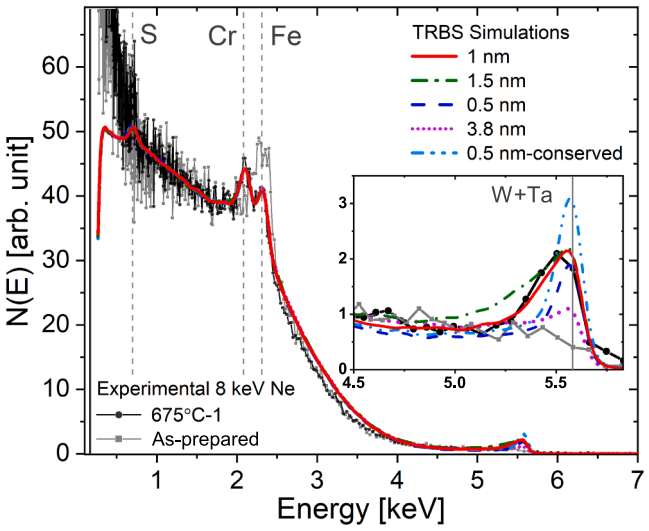

Fig. 6. TRBS simulations and experimental data recorded after first annealing to 675°C (675°C-1), and for the as-prepared surface, using 8 keV Ne projectiles. TRBS "1 nm" shows the most compatible simulation with a W + Ta enriched layer of 1 nm at the surface after the 675°C-1 step. TRBS "0.5 nm" and "1.5 nm" indicate structures with 0.5 and 1.5 nm first enriched layers, respectively, without preserving the excess number of W + Ta atoms/cm^2 from TRBS "1 nm". TRBS "3.8 nm" presents only one W + Ta enriched layer of 3.8 nm, and TRBS "0.5 nm-conserved" shows a composition with the first enriched layer of 0.5 nm, by preserving the excess number of W + Ta atoms/cm^2. Further details of the simulations can be found in Table 1.

observable energy range mainly unaffected by multiple scattering from Fe, i.e. above 4.5 keV detected ion energy.

The different simulations for 0.5 nm thickness and the most compatible one also illustrate that the excellent match for a thickness around 1 nm cannot be an artifact of detector resolution. In other words, if the experimental W + Ta peak was as thin as in e.g. TRBS simulation "0.5 nm" and the measured depth resolution was poorer than the simulation, the experimental peak is expected to be broadened symmetrically in the back and front edge. This observation agrees with earlier demonstrations of the achievable depth resolution of the ToF-LEIS method [12] where it has been demonstrated that thicknesses of 1, 2, 4 and 8 Å of deposited Au films are clearly resolvable in the energy converted ToF-LEIS spectra.

Another observation, which can be made, is that the intensity of W + Ta close to the kinematic edge for the as-prepared surface is found reduced. As the simulation "3.8 nm" suggests, even a homogeneous W + Ta concentration is expected to lead to a surface peak, which indicates a slight depletion of W + Ta in the outermost layers for the as-prepared surface, potentially due to preferential oxidation of Fe.

In Fig. 7, taking the parameters from TRBS "1 nm", "3.8 nm" and "0.5 nm-conserved", and the bulk concentrations in Table 1, SIMNRA [31] simulations for a standard RBS measurement with 2 MeV He ions, the scattering angle of 170° and a detector resolution of 15 keV are presented. A simple comparison between Figs. 6 and 7 shows the significant difference in depth resolution and structure of the surface peaks in TRBS and SIMNRA simulations. In fact, there is no difference between the SIMNRA simulations "1 nm", "3.8 nm" and "0.5 nm-conserved", which feature the same excess amount of tungsten atoms per unit area, whereas they can be distinguished in the case of TRBS simulations. This comparison emphasizes that while the W + Ta enrichment is visible even in the spectrum, RBS is not capable of resolving different scenarios that are easily distinguished in ToF-LEIS with high surface depth resolution.

Summary

A sample of EUROFER97 was sequentially annealed to different temperatures. *In-situ* measurement of the ToF-LEIS spectrum using 8 keV primary Ne ions as well as AES using 3 keV electron beam were performed after each annealing step. As a result, surface segregation of W + Ta, Cr, and S, as well as inward diffusion of W + Ta and Cr, in certain temperature regimes, were observed. The TRBS simulations indicate that, after first annealing to 675°C, an enriched layer of W + Ta and Cr exists at the surface of the sample which features a thickness of around 1 nm.

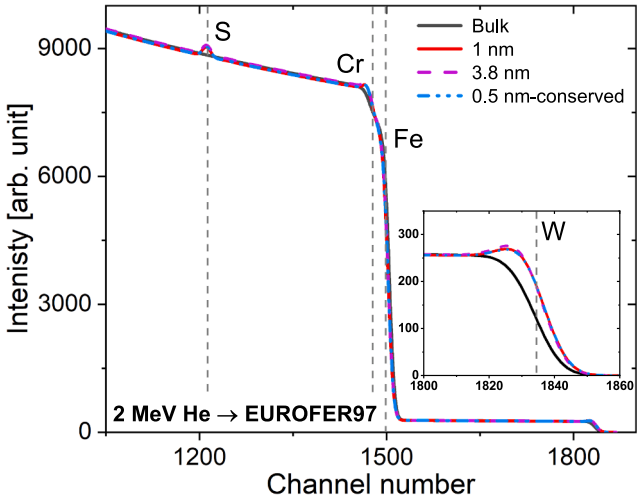

Fig. 7. SIMNRA simulations corresponding to the TRBS simulations "1 nm", "3.8 nm" and "0.5 nm-conserved", shown in Fig. 6 with the details in Table 1, compared to the bulk composition. The vertical grey dashed lines determine the position of the surface peak of each element calculated by the corresponding kinematic factors. This figure in comparison to Fig. 6 indicates that although W + Ta enrichment is visible in these simulations, RBS cannot resolve different structures which are easily distinguished in ToF-LEIS.

Table 1
Details of the compositional structure of the TRBS simulations shown in Fig. 6. EUROFER97 bulk composition is the same for all the simulations and was taken from [30]. The order of the layers from the topmost one to the bulk is as follows: layer 1, layer 2 and bulk. For more details about the density and thickness calculations see the text.

		1 nm		0.5 nm		1.5 nm		3.8 nm	0.5 nm-conserved		Bulk
		Enriched layer									
		1	2	1	2	1	2	1	1	2	
Concentrations (at.%)	**Fe**	33.5	33.5	33.5	33.5	33.5	33.5	34.39	32.3	33.5	89.34
	Cr	30.0	30.0	30.0	30.0	30.0	30.0	30.0	30.0	30.0	10.24
	W + Ta	1.8	0.6	1.8	0.6	1.8	0.6	0.91	3.0	0.6	0.42
	S	34.7	35.9	34.7	35.9	34.7	35.9	34.7	34.7	35.9	–
Density (g/cm^3)		5.8585	5.6519	5.8585	5.6519	5.8585	5.6519	5.7568	5.9956	5.6519	7.8460
Corresponding thickness (nm)		1.0	2.8	0.5	3.3	1.5	2.3	3.8	0.5	3.3	20

CRediT authorship contribution statement

Jila Shams-Latifi: Investigation, Methodology, Formal analysis, Validation, Software, Data curation, Writing – original draft, Writing – review & editing, Visualization. **Petter Ström:** Conceptualization, Methodology, Resources, Writing – review & editing, Supervision. **Eduardo Pitthan:** Methodology, Investigation, Writing – review & editing, Supervision, Project administration. **Daniel Primetzhofer:** Conceptualization, Methodology, Resources, Writing – review & editing, Supervision, Project administration, Funding acquisition.

Declaration of Competing Interest

The authors declare that they have no known competing financial interests or personal relationships that could have appeared to influence the work reported in this paper.

Acknowledgement

The authors acknowledge financial support from the Swedish research council, VR-RFI (contracts #2017-00646_9 & 2019_00191), and the Swedish Foundation for Strategic Research (SSF, contract RIF14-0053) supporting the accelerator operation. This work has been carried out within the framework of the EUROfusion Consortium, funded by the European Union via the Euratom Research and Training Programme (Grant Agreement No 101052200 — EUROfusion). Views and opinions expressed are however those of the author(s) only and do not necessarily reflect those of the European Union or the European Commission. Neither the European Union nor the European Commission can be held responsible for them. The authors would like to express their gratitude to Marek Rubel for valuable support at the initial stages of this research.

References

[1] G. Pintsuk, E. Diegele, S.L. Dudarev, M. Gorley, J. Henry, J. Reiser, M. Rieth, European materials development: Results and perspective, Sep 1, Fusion Eng. Des. (146) (2019) 1300–1307, https://doi.org/10.1016/j.fusengdes.2019.02.063.

[2] D.N. Hill, A review of ELMs in divertor tokamaks, Feb 11, J. Nucl. Mater. (241) (1997) 182–198, https://doi.org/10.1016/S0022-3115(97)80039-6.

[3] P. Ström, D. Primetzhofer, In-situ measurement of diffusion and surface segregation of W and Ta in bare and W-coated EUROFER97 during thermal annealing, Nuclear Materials and Energy. 27 (2021) 100979, https://doi.org/10.1016/j.nme.2021.100979.

[4] M. Rieth, M. Dürrschnabel, S. Bonk, S. Antusch, G. Pintsuk, G. Aiello, J. Henry, Y. De Carlan, B.E. Ghidersa, H. Neuberger, J. Rey, Fabrication routes for advanced first wall design alternatives, Oct 14, Nucl. Fusion 61 (11) (2021) 11606, https://doi.org/10.1088/1741-4326/ac2523.

[5] D. Kumar, J. Hargreaves, A. Bharj, A. Scorror, L.M. Harding, H. Dominguez-Andrade, R. Holmes, R. Burrows, H. Dawson, A.D. Warren, P.E.J. Flewitt, T. L. Martin, The effects of fusion reactor thermal transients on the microstructure of Eurofer-97 steel, Journal of Nuclear Materials. 554 (2021) 153084, https://doi.org/10.1016/j.jnucmat.2021.153084.

[6] J. Roth, K. Sugiyama, V. Alimov, T. Höschen, M. Baldwin, R. Doerner, EUROFER as wall material: Reduced sputtering yields due to W surface enrichment, Nov 1, Journal of Nuclear Materials. 454 (1–3) (2014) 1–6, https://doi.org/10.1016/j.jnucmat.2014.07.042.

[7] R. Behrisch, G. Federici, A. Kukushkin, D. Reiter, Material erosion at the vessel walls of future fusion devices, J. Nucl. Mater. 1 (313) (2003 Mar) 388–392, https://doi.org/10.1016/S0022-3115(02)01580-5.

[8] H.R. Koslowski, S.R. Bhattacharyya, P. Hansen, C. Linsmeier, M. Rasiński, P. Ström, Temperature-dependent in-situ LEIS measurement of W surface enrichment by 250 eV D sputtering of EUROFER, Aug 1, Nuclear Materials and Energy. (16) (2018) 181–190, https://doi.org/10.1016/j.nme.2018.07.001.

[9] P. Ström, P. Petersson, R.A. Parra, M. Oberkofler, T. Schwarz-Selinger, D. Primetzhofer, Sputtering of polished EUROFER97 steel: Surface structure modification and enrichment with tungsten and tantalum, Sep 1, J. Nucl. Mater. (508) (2018) 139–146, https://doi.org/10.1016/j.jnucmat.2018.05.031.

[10] D. Primetzhofer, M. Spitz, E. Taglauer, P. Bauer, Resonant charge transfer in low-energy ion scattering: Information depth in the reionization regime, Nov 1, Surf. Sci. 605 (21–22) (2011) 1913–1917, https://doi.org/10.1016/j.susc.2011.07.006.

[11] D. Primetzhofer, E.D. Litta, A. Hallén, M.K. Linnarsson, G. Possnert, Ultra-thin film and interface analysis of high-k dielectric materials employing Time-Of-Flight Medium Energy Ion Scattering (TOF-MEIS), Aug 1, Nucl. Instrum. Methods Phys. Res., Sect. B (332) (2014) 212–215, https://doi.org/10.1016/j.nimb.2014.02.063.

[12] D. Primetzhofer, S.N. Markin, P. Zeppenfeld, P. Bauer, S. Prusa, M. Kolibal, T. Sikola, Quantitative analysis of ultra thin layer growth by time-of-flight low energy ion scattering, Appl. Phys. Lett. 92 (1) (2008) 011929, https://doi.org/10.1063/1.2822816.

[13] Markin S. Electronic interaction of slow light ions with matter, Doctoral dissertation, Johannes Kepler Universität Linz, 2007.

[14] M. Draxler, S.N. Markin, S.N. Ermolov, K. Schmid, C. Hesch, A. Poschacher, R. Gruber, M. Bergsmann, P. Bauer, ACOLISSA: a powerful set-up for ion beam analysis of surfaces and multilayer structures, Mar 8, Vacuum 73 (1) (2004) 39–45, https://doi.org/10.1016/j.vacuum.2003.12.041.

[15] H.H. Brongersma, M. Draxler, M. De Ridder, P. Bauer, Surface composition analysis by low-energy ion scattering, Mar 1, Surf. Sci. Rep. 62 (3) (2007) 63–109, https://doi.org/10.1016/j.surfrep.2006.12.002.

[16] P. Ström, Material characterization for magnetically confined fusion: Surface analysis and method development, Doctoral dissertation, KTH Royal Institute of Technology (2019). http://urn.kb.se/resolve?urn=urn:nbn:se:kth:diva-241093.

[17] N. Matsunami, Y. Yamamura, Y. Itikawa, N. Itoh, Y. Kazumata, S. Miyagawa, K. Morita, R. Shimizu, H. Tawara, Energy dependence of the ion-induced sputtering yields of monatomic solids, Jul 1, At. Data Nucl. Data Tables 31 (1) (1984) 1–80, https://doi.org/10.1016/0092-640X(84)90016-0.

[18] T.T. Tran, C. Lavoie, Z. Zhang, D. Primetzhofer, In-situ nanoscale characterization of composition and structure during formation of ultrathin nickel silicide, Appl. Surf. Sci. 536 (2021) 147781, https://doi.org/10.1016/j.apsusc.2020.147781.

[19] J.F. Ziegler, M.D. Ziegler, J.P. Biersack, SRIM–The stopping and range of ions in matter (2010), Jun 1, Nuclear Instruments and Methods in Physics Research Section B: Beam Interactions with Materials and Atoms. 268 (11–12) (2010) 1818–1823, https://doi.org/10.1016/j.nimb.2010.02.091.

[20] H.J. Grabke, D. Wiemer, H. Viefhaus, Segregation of sulfur during growth of oxide scales, Apr 1, Appl. Surf. Sci. 47 (3) (1991) 243–250, https://doi.org/10.1016/0169-4332(91)90038-L.

[21] L.E. Davis, Handbook of Auger electron spectroscopy, Physical Electronics Division. (1978).

[22] A. Tolstogouzov, S. Daolio, C. Pagura, Evaluation of inelastic energy losses for low-energy Ne+ ions scattered from aluminum and silicon surfaces, Oct 20, Surf. Sci. 441 (1) (1999) 213–222, https://doi.org/10.1016/S0039-6028(99)00881-X.

[23] M. Draxler, R. Beikler, E. Taglauer, K. Schmid, R. Gruber, S.N. Ermolov, P. Bauer, Comprehensive study of the surface peak in charge-integrated low-energy ion scattering spectra, Aug 20, Phys. Rev. A 68 (2) (2003), 022901, https://doi.org/10.1103/PhysRevA.68.022901.

[24] S.P. Chenakin, R. Kolarova, S.N. Markin, D. Primetzhofer, P. Bauer, Influence of screening and electronic stopping on LEIS spectra, May 1, Nuclear Instruments and Methods in Physics Research Section B: Beam Interactions with Materials and Atoms. 258 (1) (2007) 32–35, https://doi.org/10.1016/j.nimb.2006.12.173.

[25] D. Primetzhofer, S.N. Markin, R. Kolarova, M. Draxler, R. Beikler, E. Taglauer, P. Bauer, On the surface sensitivity of angular scans in LEIS, May 1, Nucl. Instrum. Methods Phys. Res., Sect. B 258 (1) (2007) 36–39, https://doi.org/10.1016/j.nimb.2006.12.176.

[26] I.A. Vatter, J.M. Titchmarsh, Comparison of FEG-STEM and AES Measurements of Equilibrium Segregation of Phosphorus in 9% Cr Ferritic Steels, Sep 25, Surface and Interface Analysis: An International Journal devoted to the development and application of techniques for the analysis of surfaces, interfaces and thin films. (10) (1997) 760–776, https://doi.org/10.1002/(SICI)1096-9918(199709)25:10%3C760::AID-SIA298%3E3.0.CO;2-S.

[27] P. Fernandez, M. Garcıa-Mazarıo, A.M. Lancha, J. Lapena, Grain boundary microchemistry and metallurgical characterization of Eurofer'97 after simulated service conditions, Aug 1, J. Nucl. Mater. (329) (2004) 273–277, https://doi.org/10.1016/j.jnucmat.2004.04.055.

[28] J.P. Biersack, E. Steinbauer, P. Bauer, Nucl. Instrum. Methods Phys. Res. B61 (1991) 77.

[29] W. Takeuchi, Evaluation of screening length corrections for interaction potentials in impact-collision ion scattering spectroscopy, Oct 15, Nucl. Instrum. Methods Phys. Res., Sect. B (313) (2013) 33–39, https://doi.org/10.1016/j.nimb.2013.08.003.

[30] Technical specifications, EUROFER material database, F4E-2008-GRT-010 (PNS-MD).

[31] M. Mayer, SIMNRA user's guide, Report IPP 9/113, Max-Planck-Institut für Plasmaphysik, Garching, Germany, 1997.